Proceedings of the 20th International Conference on Soil Mechanics and Geotechnical Engineering– Rahman and Jaksa (Eds)

Numerical simulation of seismic landslide behaviors in a shaking table model test

Simulation numérique des comportements des talus sismiques dans une étude de modèle sur une table à secousses

Meei-Ling Lin, Ming-Huei Zou & Tai-Tien Wang
Department of Civil Engineering, National Taiwan University, Taiwan, linml@ntu.edu.tw

Kuo-Lung Wang
Department of Civil Engineering, National Chi Nan University, Taiwan

ABSTRACT: Due to the difficulties of monitoring in-situ seismic slope behaviors, the model tests are often used in laboratory to simulate field condition. A large-scale shaking table model slope test was conducted under a 1-g condition. The model slope was subjected to a sinusoidal simple harmonic motion with step-wise increase in amplitude. The law of similitude proposed by Meymand (1998) was referred and adopted to relate model slope to prototype slope. The failure time of the model slope was estimated according to the measured acceleration responses and images recorded. A numerical model using finite difference method was developed in this study to analyze slope behaviors of the large-scale model slope shaking table test. The failure plane and failure time were estimated from results of the numerical model analysis. The failure condition in numerical simulation was compared to the measurements of model test and consisted well for the failure development and cracks near the crest. It was found that the numerical model established according to the slope model test could be used to simulate in-situ seismic slope response observing proper law of similitude.

RÉSUMÉ : En raison des difficultés de surveillance in situ des comportements des talus sismiques, on a souvent utilisé des études sur modèle en laboratoire pour simuler les conditions en milieu réel. Un test a été réalisé avec un modèle de talus sur une table à secousse de grandes dimensions sous des conditions 1-g. Le talus modèle a été soumis à une oscillation harmonique sinusoïdale simple avec un accroissement graduel de l'amplitude. On s'est référé à, et adopté, la loi de la similitude proposée par Meymand (1998) pour représenter le talus modèle et le talus prototype. Le temps de rupture du talus modèle a été évalué en fonction des réactions d'accélération mesurées et des images enregistrées. Un modèle numérique utilisant la méthode des différences finies a été développée lors de cette étude afin d'analyser les comportements des talus modèles sur une table à secousse de grandes dimensions. Le plan de rupture et le temps de rupture ont été estimés à partir des résultats de l'analyse du modèle numérique. Les conditions de rupture de la simulation numérique ont été comparées aux mesures prises lors de l'étude sur modèle et étaient consistantes pour le développement de la rupture et les fissures à proximité de la crête. On a trouvé que le modèle numérique établi selon l'étude sur modèle du talus pouvait être utilisé pour simuler la réaction du talus sismique in situ en observant la loi de la similitude.

KEYWORDS: seismic slope behavior, shaking table test, law of similitude, numerical simulation.

1 INTRODUCTION

Due to the difficulties of monitoring slope behaviors in field when subjected to earthquake, the model tests are often used for observation of the field condition with proper simulation. The shaking table model test has been one of the most used model test for simulating field seismic slope behavior under 1-g gravity field. To properly simulate the field condition using a model test, the law of similitude and detailed analysis are required. Lin and Wang (2010) conducted a large-scale model slope shaking table test using the shaking table of the National Center for Research on Earthquake Engineering under 1-g gravity field in 2009. The law of similitude was adopted to relate model slope to prototype slope. Accelerometers were imbedded in the model slope to monitor the motion of the slope body during the test, and a digital video recorder (DV) was used to record images of the slope deformation and displacement. The failure time of the model slope was estimated according to the measurements of acceleration responses and analysis of DV images. However, the failure mechanism and slope behaviors could not be thoroughly understood and analyzed based on the measured responses and images only. In order to understand the seismic slope behavior during the shaking table model test, a numerical model was constructed using finite difference method in this study. The slope behaviors and failure plane from the numerical model were then compared to the measured acceleration responses and observed displacement of the model slope. The seismic slope behaviors observed in model test were then discussed comparing to the numerical simulation.

2 SHAKING TABLE SLOPE MODEL TEST

Lin and Wang (2010) conducted a 1-g large-scale model slope shaking table test in 2009. The shaking table of the National Center for Research on Earthquake Engineering has a dimension of 5m by 5m and six degrees of freedom with a pay load of 50 tons. The model box used for encasing model slope was a rigid-walled box having an inner length of 4.4m, a width of 1.3m, and a height of 1.2m. A preliminary numerical analysis was performed to determine the proper layout including boundary and base layer of the model slope to avoid the boundary effects during the test (Lin and Wang 2006). The constructed model slope has a height of 0.5m and a base layer thickness of 0.3m. The slope situates at the center section of the box with sufficient distances from the box walls. In addition, the box walls were lubricated with silicon oil and thin plastic films to minimize the boundary effects.

We used a uniform fine sand for construction of the model slope. The composition of the sand is mainly silicon, and specific gravity of the sand is 2.66. The model slope was constructed by pluviating dry sand from a given height into the model box to a layer thickness of 10cm, and the process was repeated till

reaching a total layer thickness of 80cm. The slope was formed by excavation while maintaining a slope angle of 30◦, and the final slope height was 50 cm. The slope thus formed has an initial mass density of 1539.4 kg/m^3 and a relative density of 61% based on the data during construction process of the model slope. Figure 1 shows the side view of the constructed model slope. Instrumentations including accelerometers and linear variable differential transformers (LVDT) were deployed to monitor the motion of the model box and model slope. The displacement and deformation of the slope surface were recorded using a digital video recorder during the loading process. The accelerometers were placed near the slope surface every 10 cm apart vertically from the base up following pluviation of each sand layer. Additional accelerometers were placed at the corners of the model box and top of shaking table to record motions of the box and table for comparisons. The LVDTs were set up at the four corners of the model box to measure the horizontal displacements in the direction of shaking. The DV was set up perpendicular to the model slope surface to record the images of slope displacements and crack development. Layout of the instrumentation of the model slope is illustrated in Figure 2.

Figure 1. Side view of the constructed model slope in the model box.

Figure 2. Layout of instrumentation including accelerometers, LVDTs, and DV in the constructed model slope and model box.

In order to relate the field condition to the model test, the

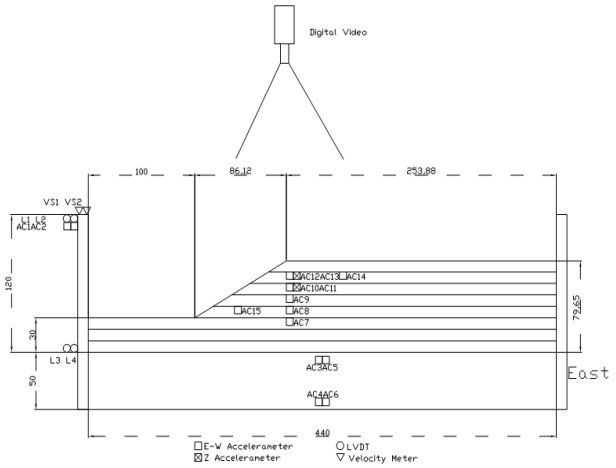

requirement of similitude need to be satisfied. The requirements of similitude include: geometry similitude, kinematic similitude, and dynamic similitude (Langhaar 1951). To derive the similitude requirement, the dimension analysis method can be used (Kline 1965). Iai (1989) utilized governing equation and constitutive law to derive the law of similitude for 1-g shaking table model test for saturated soil-structure-fluid model. Meymand (1998) derived the similitude relation following the model test conditions of: (1) the accelerations of the model and prototype remained the same under 1-g field; (2) the soil mass densities were the same for the model and proto-type; and (3) the undrained soil strengths were not affected by the confining pressure. When adopting the same assumptions into the law of similitude by Iai (1989), the scaling factors can be reduced to the same results as those in Meymand (1998). Lin and Wang (2010) assumed a proto-type slope with a slope height of 10m, and being subjected to a sinusoidal simple harmonic ground motion with a frequency of 2 Hz. Considering the similar testing conditions, the law of similitude proposed by Meymand (1998) was referred and the scaling factors between the prototype slope and model slope were derived using dimension analysis method. Based on the geometry ratio of 20 between slope heights of prototype slope and model slope, the parameters derived observing the law of similitude were listed in Table 1. For a field motion frequency of 2 Hz, the frequency of motion to be applied to the model slope will be 8.9 Hz to satisfy the law of similitude as shown in Table 1. We then used a sinusoidal wave with a frequency of 8.9Hz as the input acceleration motion in the horizontal direction of the shaking table. The amplitude of the motion increases sequentially in step-wise form from 0.05g, 0.1g, 0.2g, 0.3g, up to 0.5g, with loading cycles of 7, 35, 35, 35, and 40, respectively. The loading amplitude of 0.05g was applied as a pre-shaking with very low amplitude and few cycles only. The input loading history is as shown in Figure 3. The model slope gradually became denser as the loading process proceeded. The samples taken after final loading stage of the model slope have an average relative density of 94.5% and an average mass density of 1618.97 kg/m^3.

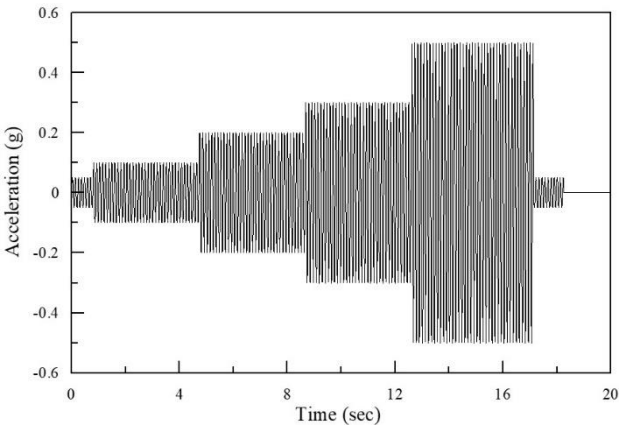

Figure 3. Time history of the loading amplitude of the input motion.

Table 1. Parameters of prototype slope and model slope observing the law of similitude

Parameter	Prototype slope	Model slope
Unit weight (kN/m^3)	15.1	15.1
Acceleration (g)	1	1
Slope height (m)	10	0.5
Base layer thickness (m)	6	0.3
Frequency (Hz)	2	8.9
Strain ratio	1	1

3 NUMERICAL MODEL FOR SEIMIC SLOPE ANALYSIS

We adopted the finite difference method for construction of the numerical model for analysis of seismic slope behavior using a commercially available software FLAC (Fast Lagrangian Analysis of Continua, FLAC 2005). The Mohr-Coulomb failure criterion was assumed for the material properties, and geometry of the numerical model slope was the same as the shaking table model slope. The size of the mesh grid used for the numerical analysis was determined based on the dynamic properties of soil, geometry of slope, and wave length from soil property and motion frequency. The gravity force was applied to the numerical model slope with the lateral boundaries fixed in the horizontal direction, and the base boundary fixed in both the horizontal and vertical directions. When reaching static equilibrium condition, the model slope would be subjected to the initial static stress field. The resulting stress distribution confirmed that the geometry of the model slope suggested negligible boundary effects (Lin and Wang 2006). The box was assumed to be relative stiff compared to the stiffness of the testing soil, and the kinematic boundary was adopted for the seismic slope behavior analysis. Study by Wang and Lin (2011) confirmed that the kinematic boundary was proper for the layout of the model slope, and thus the kinematic boundary was applied to both the lateral and base boundaries. A comparison study was conducted in this study for different types of input motion for the kinematic boundary. It was found that the velocity motion input with the base line correction would provide a better interpretation for the slope responses. Thus, the acceleration loading time record in Figure 3 was integrated to obtain the velocity loading record, and then the baseline correction was conducted (Boore 2001, Chiu 1997). The input motion at the kinematic boundary of the numerical model utilized this corrected velocity loading sequence. Figure 4 shows the grid mesh and the kinematic boundary of the numerical model slope.

Figure 4. The grid mesh and kinematic boundary of the numerical model, the dimensions are in m.

The properties of the same sand used in the model slope has

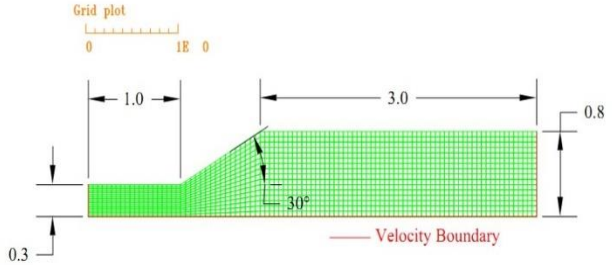

been used and tested in several studies previously (Zheng 2006, Lin 2007, Chen 2010, and Hsu 2010). A correlation of friction angle versus relative density of the sand could be determined from summarizing data of previous studies as:

$$\phi' = 0.0791 \times Dr + 31.485 \quad (1)$$

where ϕ' is the effective stress friction angle in degree, and D_r is the relative density of the sand. The model slope was with a medium relative density initially, but as the loading amplitude proceeded, the model slope became denser and its relative density increased gradually. The constant soil properties were used in the numerical model analysis. To ensure proper simulation of the seismic slope behavior while approaching higher loading amplitude and failure condition, the relative density determined after the last loading stage was used. The friction angle thus determined was 39°, and a dilation angle of 10° was used. The initial shear modulus of the sand was estimated using the correlation proposed by Hardin and Drnevich (1972):

$$G_0 = 3230 \frac{(2.973-e)^2}{(1+e)} (\sigma'_{mean})^{0.5} \quad (2)$$

in which G_0 is the initial shear modulus in kPa, e is the void ratio, and σ'_{mean} is the average effective stress in kPa. The average effective stress was computed based on the stress generated after the static equilibrium of the numerical model slope in 1-g gravity field. The average stress of elements near the slope was computed, and the initial shear modulus could be determined accordingly. Table 2 shows the parameters used in the numerical analysis.

Table 2. Parameters used in the numerical model

Parameter	
Density (kg/m^3)	1618.97
Bulk modulus K (MPa)	58.67
Shear modulus G (MPa)	27.08
Cohesion (MPa)	0
Tensile strength (MPa)	0
Friction angle ϕ' (°)	39.0
Dilation angle ψ (°)	10
Poisson's ration ν	0.3
Minimum frequency f_{min} (Hz)	5
Minimum damping ratio ξ_{min} (%)	0.74

4 RESULTS OF MODEL TEST AND NUMERICAL ANALYSIS

The slope behaviors in the model test were monitored using the accelerometers and digital video images. The responses of the model slope are presented using the acceleration records of the AC12, which located near the crest and slope face of the model slope as shown in Figure 2. Figure 5 shows the acceleration responses of the model slope at AC12 taking positive sign in the up-slope direction. Observing the acceleration time record, the slope response is about synchronized with the input motion without obvious phase shift for loading amplitudes of 0.1g, and 0.2g. This suggested a linear elastic behavior of the model slope for the first two loading amplitudes. However, the acceleration amplitudes measured by AC12 appeared to be larger than the input motion amplitude in Figure 3, and the acceleration amplitude records of AC7 located at the elevation of toe of the slope as shown in Figure 6. This might be caused by the amplification effects for AC12 located near the slope crest and at higher elevation compared to the base and toe of slope. When motion amplitude increased to 0.3g, the response of AC12 appeared to be almost linear, but some nonlinear response occurred at later stage as the loading time increased to about 11.7sec. A similar response trend could be found in AC7 response record but not as significant as in response record of AC12. When loading amplitude increased to 0.5g, a significant

nonlinear response occurred in AC12 record, and the motion of the slope appeared leaning toward the down-slope direction

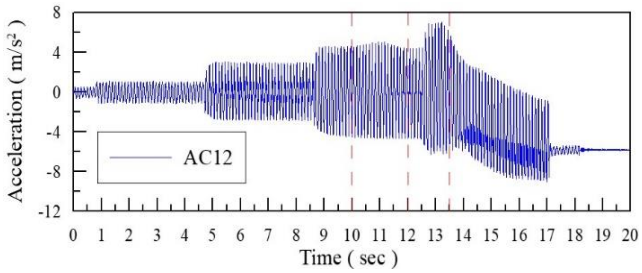

Figure 5. The acceleration records at AC12 near the crest of the model slope.

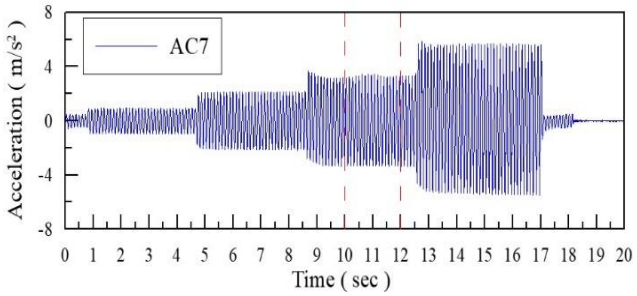

Figure 6. The acceleration records at AC7 at the toe level of model

continuously before 13.5 sec. The nonlinear behavior was indicated by non-uniform and non-symmetric response amplitude comparing Figure 5 to Figure 6 following the marked time line. This comparison also showed phase shift of response motion, and similar phase shift was also found when comparing the response to the input motion. Thus, it was speculated that a main sliding of slope body might have initiated at 11.7sec. with 0.3g loading amplitude, however, the displacement might be small. The slope failed significantly with the 0.5g loading amplitude from the response motion records, and caused a sliding motion toward the down slope direction. The shifting of the AC12 response toward the down slope direction also suggested a significant displacement at AC12 that might have caused the accelerometer to shift, and the smaller amplitude suggested a possible development of shear zone in the slope.

The time frames of the images taken by the DV were synchronized with loading sequences, and the frames corresponding to peak of loading amplitudes were selected for inspection and analysis. No significant disturbances or cracks were observed for the loading amplitudes of 0.1g and 0.2g. However, some small-scale movements on the slope surface were recorded. These movements appeared to be superficial and local without causing significant movement of the main slope body as shown in Figure 7. When the loading amplitude increased to 0.3g, the frontal part on the slope crest started to displace at about 11.7 sec., but no significant cracks or deformation of the slope body were observed. The timeline of this displacement corresponded to the response record of AC12 well in Figure 5, when development of nonlinear motion initiated. A visible crack developed on the slope crest, and the nearest distance of the crack to the edge of crest was about 8.3 cm from the image at time frame of 13.5 sec. and with the loading amplitude of 0.5g. Following the crack development, crest and toe of the model slope appeared to displace toward the downslope direction, and a massive movement of the slope occurred as shown in Figure 8 with a significant sign of crown subsidence. Comparing the time line for crack development to the motion record of AC12, a significant nonlinear downslope motion was obvious and coincided well with the image observation.

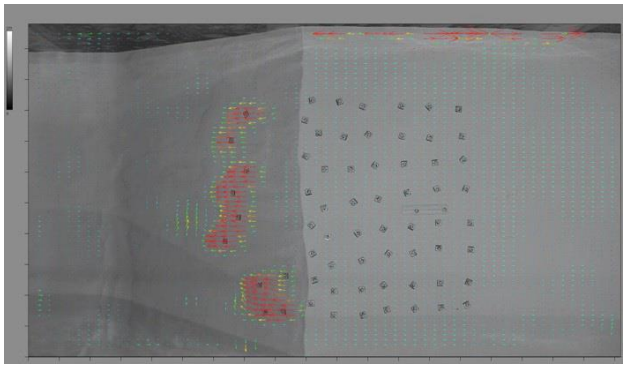

Figure 7. Images taken for loading amplitude of 0.1g. The red color arrow indicates the detected movement toward the down slope direction based on results of image analysis.

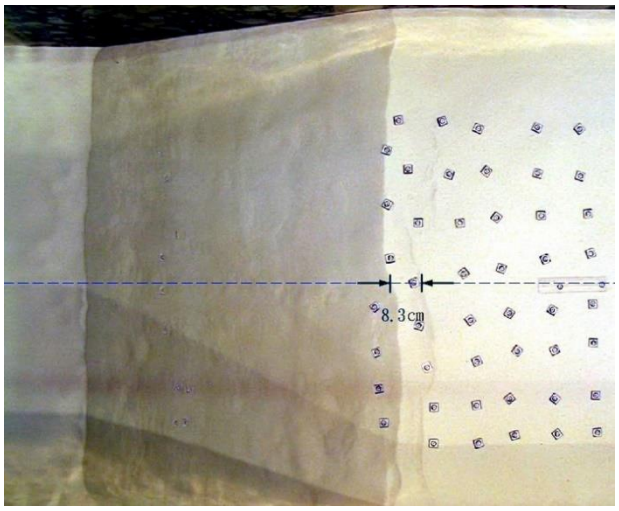

Figure 8. Images taken for loading amplitude of 0.5g, and the nearest distance of the visible crack to the edge of crest was about 8.3 cm. Displacements on the slope surface, crest, and at toe can be observed.

Results of the numerical model simulation were examined following each loading amplitudes and time line. Figure 9 shows the distribution of the shear strain of the slope with the loading amplitude of 0.1g. It was found that the shear strain of the slope was smaller than 10^{-4} for the loading amplitude, and most part of the slope behaved elastically as shown in Figure 9. However, shear strain for the elements near the slope surface appeared to have a much larger value. This shear strain distribution near the slope surface coincided well with the superficial displacement observed in digital images in Figure 7. This result confirmed that the displacement zone was superficial only, and would not affect the main slope body. Figure 10 shows the distribution of shear strain of the slope when the loading amplitude increased to 0.3g at 11sec. Observing Figure 10, a shear zone developed at a greater depth extending through the whole slope body with a circular shape, and a separate shallow shear zone also developed near the slope surface. This suggested that a deep-seated circular shape sliding occurred, and some superficial displacements near the slope surface also occurred at about 11sec. Figure 11 shows the shear surface estimated based on the distribution of the maximum shear strain increment at 11 sec., and the outcrop of shear surface on the crest located at about 11 cm from the edge of the crest.

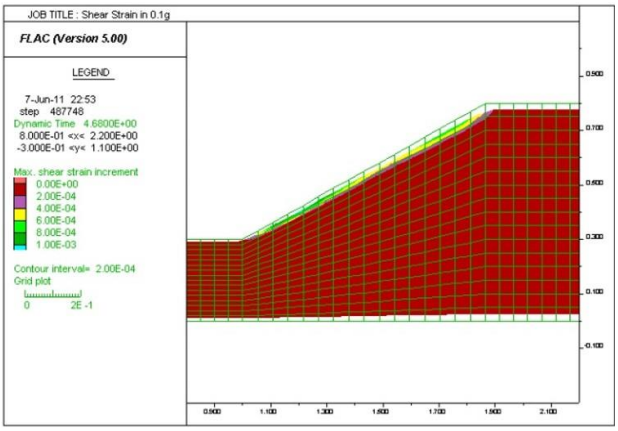

Figure 9 Distribution of shear strain of the numerical model slope for loading amplitude of 0.1g. Larger shear strain distributed near the slope surface suggesting superficial displacements with main part of slope remained elastic.

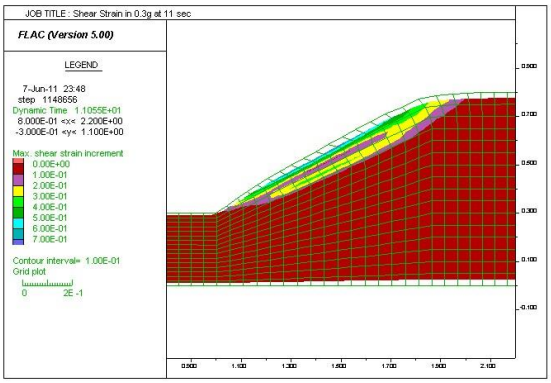

Figure 10. Distribution of shear strain of the numerical model slope for loading amplitude of 0.3g. A shear zone with a circular shape developed at a greater depth and extended through the slope body, and a separate shallow shear zone developed near the slope surface.

5 DISCUSSIONS

Based on the monitored motion responses during the test, the slope behaved elastically during the loading amplitudes of 0.1g and 0.2g, and the response motions were in-phase with input motions. From the recorded images of DV, some superficial displacement occurred on the slope face, but no displacement was observed near the crest or toe at these loading amplitudes. This superficial displacement appeared to be local, and did not affect the overall slope behavior, and thus was not registered by the accelerometers. Comparing the monitored results to the numerical analysis, the superficial displacement started to appear in the numerical simulation result when amplitude reached 0.1g in Figure 9, and confirming that the main slope body was not affected. For loading amplitude of 0.3g, the nonlinear response initiated at 11.7sec from the motion record of AC12, however, no significant displacement was observed in the DV images. This might suggest the initiation of landslide, but the accumulated displacement might still be small without causing significant sliding behavior. From the numerical analysis results, the distribution of the shear strain suggested that the landslide initiation occurred with loading amplitude of 0.3g at about 11sec. in Figure 10, which consisted with the observed nonlinear motion response well. In addition, the superficial displacement on the slope surface was observed, and appeared to occur simultaneously for loading amplitude of 0.3g in Figure 10. Due to the limitation of the numerical model in analyzing large displacement, we did not conduct numerical analysis for the loading amplitude of 0.5g. The potential sliding surface was estimated from the maximum shear strain increment with the scarp located at a distance of about 11 cm from the edge of crest in Figure 11. Location of this scarp compared well with the location of crack observed in Figure 8, where the distance of 8.3 cm showed the distance of the narrow part of crack after the test. The initiation time line of the overall slope sliding was not so obvious in the acceleration response records and could not be detected from the DV images at this time. However, the numerical model appeared to provide insight into the initiation of slope sliding before significant displacement could be observed from the monitored data of model slope, and the shear surface could be determined. Results of the numerical analysis in this study provided consistent results compared to the acceleration responses observed and recorded images of the model test, and were able to interpret the slope behaviors more into details and confirmed the estimations from the monitored results. Thus, the properly set-up numerical model could provide more details into the responses and interpretation of the model test results, and to further understand the seismic slope behavior.

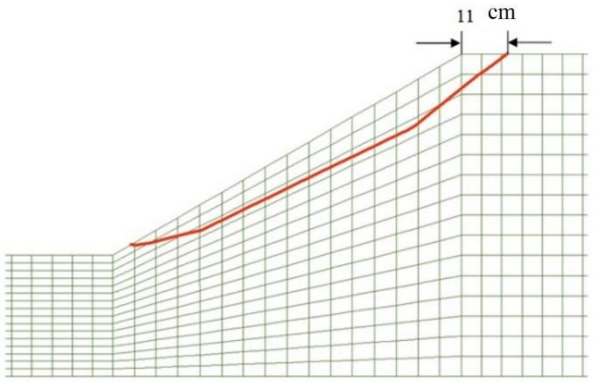

Figure 11. The shear surface estimated from the distribution of the maximum shear strain increment at 11 sec., and the outcrop of shear surface on the crest located at about 11 cm from the edge of the crest

6 CONCLUSIONS

Due to the difficulties of monitoring in-situ seismic slope behaviors, the model tests are often used in laboratory to simulate field condition. A large-scale shaking table model slope test was conducted under a 1-g condition and adopting the law of similitude. The failure condition and corresponding timeline of the model slope was estimated according to the measured acceleration response records and images recorded. The numerical model was developed to simulate seismic behaviors and analyze the failure mechanism of the model slope. The numerical model results provided shear strain distribution and corresponding timeline over the whole loading sequences. Superficial displacement was observed in the monitored images when the loading amplitude was 0.1g, and results of the numerical model confirmed this behavior with the distribution of shear strain and showing no significant deformation of the main slope body. It suggested that the superficial displacement was local, and did not affect the overall stability of the model slope. For the overall sliding of model slope, the failure condition in numerical simulation was at amplitude of 0.3g, while minor sign of nonlinear response was measured at 11.7 sec. Thus the numerical model provided supporting information for initiation of sliding behavior. The failure surface determined from the numerical model was in good agreement with the cracks and

subsidence near the crest recorded by images. Thus, the properly set-up numerical model could provide more detail information and better interpretation of the seismic responses of the model test results, and thus improve understanding of the seismic slope behaviors.

7 ACKNOWLEDGEMENTS

This research was supported by the National Science Foundation, Taiwan, project number: NSC97-2221-E-002-190.

8 REFERENCES

Boore D. M. 2001. Effect of baseline corrections on displacements and response spectra for several recordings of the 1999 Chi-Chi, Taiwan, earthquake*, Bull. Seism. Soc. Am.* 91, 1199-1211.

Chen Y. S. 2010. *Simulation of landslide using small-scale shaking table*, MSc. Thesis, National Taiwan University, Taiwan.

Chiu, H. C. 1997. Stable baseline correction of digital strong-motion data, *Bull. Seism. Soc. Am.* 87, 932-944.

FLAC v5.0 manual 2005, Itasca.

Hardin B. O. and Drnevich V. P. 1972. Shear modulus and damping in soils: design equations and curves, *Journal of the soil mechanics and foundations division, ASCE*, 98(SM7), 9006, 667-692.

Hsu S. Y. 2010. *Simulation of seismic slope behavior using model test*, MSc. Thesis, National Taiwan University, Taiwan.

Iai S. 1989. Similitude for shaking table tests on soil-structure-fluid model in 1g gravitational field, *Japanese Society of Soil Mechanics and Foundation Engineering*, 29 (1), 105-118.

Kline S. 1965. *Similitude and Approximation Theory*, McGraw-Hill, New York

Langhaar H. 1951. *Dimensional analysis and theory of models*, John Wiley and Sons, New York.

Lin J. H. 2007. *A numerical simulation of landslide induced by earthquake*, MSc. Thesis, National Taiwan University, Taiwan.

Lin M. L. and Wang K. L. 2006. Seismic slope behavior in a large-scale shaking table model test. *Engineering Geology* 86, 118-133.

Meymand P. J. 1998. *Shaking table scale model tests of nonlinear soil-pile-superstructure interaction in soft clay*, Ph. D. dissertation, U. C. Berkeley.

Wang K. L. and Lin M. L. 2010. Seismic slope behavior of a large-scale model slope under 1-g condition, *Sino-Geotechnics*, 125, 23-34.

Wang K. L. and Lin M. L. 2011. Initiation and displacement of landslide induced by earthquake - a study of shaking table model slope test. *Engineering Geology,* 122, 106-114

Zheng, S. J. 2006, *Simulation of slope subjected to earthquake using a small-scale shaking table test*, MSc. Thesis, National Taiwan University, Taiwan.